THE JOURNAL OF PHYSICAL CHEMISTRY C

Article

pubs.acs.org/JPCC

Mechanisms of Oxidation of $NdNiO_{3-\delta}$ Thermochromic Thin Films Synthesized by a Two-Step Method in Soft Conditions

A. Boileau,[†] F. Capon,[*,†] P. Laffez,[‡] S. Barrat,[†] J. L. Endrino,[§] R. Escobar Galindo,[∥] D. Horwat,[†] and J. F. Pierson[†]

[†]Université de Lorraine, Institut Jean Lamour, Département CP2S, UMR CNRS 7198, Parc de Saurupt, Nancy F-54011, France

[‡]Université François Rabelais de Tours, Groupe de Recherche Electronique, Matériaux, Acoustique, Nanoscience (GREMAN), UMR CNRS 7347, IUT de Blois, 15 rue de la Chocolaterie, Blois F-41000, France

[§]Abengoa Research S. L., Abengoa, Campus Palmas Altas, Seville E-41014, Spain

[∥]Instituto de Ciencia de Materiales de Madrid, ICMM-CSIC, Campus Cantoblanco, Madrid E-28049, Spain

ABSTRACT: Considering it is somewhat difficult to crystallize thermochromic nickelates through a soft process, a major challenge in $NdNiO_3$ crystallization is the stabilization of the Ni^{3+} oxidation state against Ni^{2+}. The aim of the present work was to understand why a soft annealing is sufficient while an oxygen high pressure (200 bar) is usually considered as required. Thin films of 300 nm have been deposited by reactive magnetron sputtering at room temperature and working pressure of 0.5, 4, and 7 Pa. The oxygen content of as-deposited and annealed films was estimated by Rutherford backscattering spectrometry, whereas the nickel oxidation state evolution was followed by X-ray photoelectron spectroscopy. The measurements showed that the Ni^{3+} state is reached after deposition whatever the deposition pressure but that an oxygen loss occurs during air annealing with a magnitude depending on the deposition pressure. X-ray diffraction measurements, four-point probe electrical measurements, and infrared optical properties vs temperature were consistent with these results. Thin films deposited at 0.5 Pa and annealed in air at 820 K lead to an orthorhombic structure which becomes rhombohedral when the deposition pressure reaches 7 Pa. The oxygen loss causes a deterioration of the electrical resistivity, which was also evidenced by the thermochromic behavior measured using Fourier transform infrared spectroscopy.

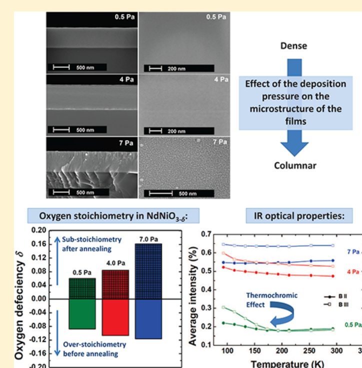

I. INTRODUCTION

Nowadays, thermochromic oxides open numerous smart applications such as temperature-modulated switches, sensors, or thermochromic coatings, if deposited as thin films over an appropriate substrate. Among them, VO_2,[1−3] $NdNiO_3$,[4,5] and recently manganites[6,7] and cobaltites[8] own high capabilities to modulate an infrared radiation. Over the past two decades, the $ReNiO_3$ (Re = La, Pr, Nd, Sm, ...) nickelates have been intensively studied for their thermochromic properties as bulk perovskites and thin films. Furthermore, solid-state rare earth mixtures ($Re_{1-x}Re'_xNiO_3$) lead to an easy tuning of the optical transition based on a metal−insulator transition (MIT) versus temperature in the infrared range, according to the nature of the rare earth element substituted into the perovskite structure.[9,10] For example, $Sm_{0.37}Nd_{0.63}NiO_3$ and $Nd_{0.7}Eu_{0.3}NiO_3$ nickelates show an optical transition at room temperature,[9,11] whereas $NdNiO_3$ undergoes a MIT at 200 K.[12] Concerning VO_2, it undergoes an abrupt phase transition at 341 K. Various ions have been used to dope VO_2 thin films to reduce the transition temperature, but they are known to affect nanoscale phase transitions. Moreover, the diversity of the oxidation state of vanadium in vanadate compounds[13] leads to nonthermochromic parasite phases (such as V_2O_3, V_6O_{13}, V_2O_5) often remarked[14−16] and requires attentive synthesis conditions in the perspective of industrial developments.

Besides, the optical band gap of $NdNiO_3$ (0.10 eV)[11] is smaller than $Sm_{0.5}Ca_{0.5}MnO_3$ (0.71 eV)[7] and VO_2 (1.81 eV)[17] that ensures the entire opacity of the material in the visible part of the spectrum. Regarding $NdNiO_3$ coatings, in most studies, the research is focused on the electrical properties driven by the epitaxial growth on relevant substrates (also known as substrate effect), the residual stresses, the film thickness, or the nature of the rare earth element used.[18] In contrast, the effect of the oxygen content on the electrical behavior in thin films and bulk samples has been less discussed. Tiwari et al.[19] and Nikulin et al.[20] showed that small changes in oxygen stoichiometry of $NdNiO_{3-\delta}$ synthesized using the nitric method can significantly affect the electrical properties. Indeed, the oxygen content is a key point since it is involved in the electrical conduction mechanisms. A decrease in the amount of oxygen leads to a drastic deterioration of the semiconducting state and reduces the resistivity jump on both sides of the MIT. On that account, a drastic oxidation treatment subsequent to the synthesis is

Received: November 13, 2013
Revised: February 24, 2014
Published: February 24, 2014

ACS Publications © 2014 American Chemical Society

often required due to the ionization energy needed to form Ni^{3+}, which is equal to 54.9 eV compared to 35.19 eV for Ni^{2+}.[21] The Ni^{3+} oxidation state is somewhat difficult to achieve, and in any synthesis routes the major challenge is the stabilization of the Ni^{3+} oxidation state against Ni^{2+}.[22] Regarding nickel oxide stability, it is widely known that NiO is oxidized to Ni_2O_3 by absorbing oxygen at around 670 K, and then it is reduced to NiO at 870 K by oxygen desorption.[23] In 2009, Napierala et al.[24] have shown that in the bulk $Sm_xNd_{1-x}NiO_3$ parent compounds a reduction process occurs through two consecutive steps at 620 and 720 K associated to the nickel reduction as follows: $Ni^{3+} \rightarrow Ni^{2+} \rightarrow Ni^0$. To crystallize the $NdNiO_3$ perovskite structure during annealing, the temperature has to be increased up to 870 K. As a consequence of the natural tendency of Ni^{3+} to reduce at such temperature at atmospheric pressure, its stabilization in the crystalline state of $NdNiO_3$ is achieved by using high oxygen pressure.[18] Radiofrequency (RF) sputtering has been applied as a method of choice to synthesize thin $NdNiO_3$ films. An annealing treatment under tough conditions—high temperature and high oxygen pressure (up to 970 K and 200 bar, respectively)—was usually used to achieve and maintain the Ni^{3+} oxidation state and thus to crystallize orthorhombic perovskite structure with thermochromic properties. DeNatale et al.[25] synthesized $NdNiO_3$ films on $LaAlO_3$ by RF magnetron sputtering. The process consisted of a sputtering step at 870 K followed by an annealing step at 1220 K under 117 bar of oxygen. In the same way, Escote et al.[26] reported an electrical switch in $NdNiO_3$ thin films elaborated by RF sputtering in argon atmosphere at room temperature and a subsequent heat treatment close to 870 K under 60 bar of oxygen. Thin films deposited by this method at room temperature were found amorphous, and heat treatment under high oxygen pressure was required.[11,27] Under these conditions, polycrystalline films were formed, which exhibited a MIT around 150 K. The influence of the substrate temperature has been investigated by Laffez et al.[28] Deposited at 870 K, thin films crystallize in situ in an oriented isotype structure (Nd_2NiO_4, NiO) in which the oxidation state +3 of the Ni ions is not reached. The preferential formation of Ni^{2+} at high temperature can be attributed to the nonthermodynamic equilibrium conditions of Ni^{3+} instantly destabilized to Ni^{2+}. An oriented $NdNiO_3$ perovskite structure was solely formed after a postannealing at 1220 K under 200 bar of O_2. Resulting electrical properties exhibited a transition temperature around 200 K, as usually observed in bulk ceramics.

To avoid such a drastic process, different routes such as metal−organic chemical vapor deposition[29,30] or pulsed laser deposition[31,32] are used to stabilize through epitaxial growth of the $NdNiO_3$ structure on perovskite-type substrates such as $LaAlO_3$, $SrTiO_3$, or $NdGaO_3$. Unfortunately, this approach strongly limits the possibilities of applications.

Using the sol−gel routes, Napierala et al.[33] have shown recently the possibility to synthetize a fully oxidized perovskite by using polymeric precursor associated with moderate pressure annealing (20 bar) at 1060 K. Analyses by transmission electronic microscopy led to the conclusion that the structure commonly obtained at 175 bar is perfectly observed in the sample prepared at 20 bar without major structural defects. The two types of samples (175 and 20 bar) exhibited equivalent thermochromic behavior and thermo-optical properties. Therefore, this study aims to confirm that annealing conditions required to stabilize the perovskite phase can in some cases be softer than standardly admitted, and they may be reviewed and even reduced.

We have shown in a previous study[34] the timeliness to prepare thermochromic $NdNiO_{3-\delta}$ thin films by reactive magnetron direct current (DC) cosputtering deposition followed by a soft postdeposition annealing under ambient air at 910 K. The electrical resistance and infrared (IR) optical transmittance versus temperature show interesting characteristics which are close to polycrystalline $NdNiO_3$ thin films postannealed under high oxygen pressure. The metal−insulator jump reaches 1.4 orders of magnitude and leads to an optical transmittance transition close to 20% in the 10−25 μm wavelength range. Thus, while avoiding a drastic annealing condition or epitaxial stabilization, a thermochromic thin film was synthesized on the Si substrate. These results represent a great improvement in the spread use of this thermochromic material and the possibility to work on a large substrate scale using a high deposition rate. This is expected to stimulate extensive research on $ReNiO_3$ materials, but the stabilization mechanism is not fully understood considering that these soft annealing conditions cannot explain alone the full oxidation of nickel to Ni^{3+}. To emphasize the influence of the process on the Ni^{3+} stabilization expected during the condensation species over the substrate, in this paper we investigate the effect of the working pressure imposed during the deposition step. The films have been deposited at three different working pressures and annealed in air at 820 K. X-ray diffraction (XRD) and scanning electron microscopy (SEM) analyses have been used to characterize the structural properties. The oxygen content in our films and the oxidation state of the Ni ion have been appraised from Rutherford backscattering spectrometry (RBS) and X-ray photoelectron spectroscopy (XPS), respectively. Finally, the MIT is tracked by DC electrical measurements and infrared optical characterizations vs temperature.

II. EXPERIMENTAL SECTION

The Nd−Ni oxide films have been deposited on double-side polished intrinsic {100} oriented of 300 μm thick silicon substrates. Thin coatings of 300 nm thickness were obtained by the magnetron cosputtering process from Nd and Ni metallic targets (50 mm in diameter and 3 mm and 1 mm in thickness, respectively) in $Ar-O_2$ reactive gas mixtures as described in a previous work.[34] The silicon substrates are successively cleaned in acetone and methanol activated by an ultrasonic bath and directly positioned on a rotating substrate holder positioned at 70 mm away from the metallic targets. A cylindrical vacuum reactor was used for the experiments and pumped down to a base pressure below 10^{-5} Pa by a combination of turbomolecular and rotary pumps. The gases used were a variable mixture of Ar and O_2 varying the working pressure inside the deposition chamber. To carry out this study, three different deposition pressure domains have been used. The first domain was defined at 0.5 Pa and corresponds to the lower pressure available by the suction system. This pressure range allowed by the magnetron effect is generally used to provide dense thin films.[35,36] In contrast, the second domain has been defined by the upper limit of the pumping limit near 7 Pa. Finally, an intermediate pressure around 4 Pa has been chosen. The working pressure (P_w) was regulated by a throttle valve between the chamber and the suction system. The atomic ratio Nd/Ni was adjusted according to the discharge current applied to the targets with Advanced Energy generators—DC supply on Ni and pulsed DC Pinnacle+ supply on Nd—for each

pressure range. The sputtering parameters (average power dissipated, voltage) of each target were read on the front panel of each supply. The pulsed unipolar DC power supply connected to the Nd target was operated at a frequency of 50 kHz with a duty cycle of 20%. In practice, the current applied to the Nd target was fixed at 1 A, while the current applied to the Ni target was tuned to match the atomic ratio Nd/Ni of 1 in the as-deposited films. This metal atomic ratio within the films was checked using a Phillips FEG-XL30S scanning electron microscope (SEM) equipped with an energy-dispersive spectroscopy (EDS) system. Thus, the corresponding current applied on the Ni target was fixed at 0.21, 0.39, and 0.40 A for P_w of 0.5, 4, and 7 Pa, respectively.

The optimization of the gas flow rates is a necessary step to ensure that the reactive oxidizing conditions are implemented during the sputtering process. In practice, the oxygen flow rate was gradually incorporated to 21 sccm argon keeping constant the throttle valve of the pressure regulation. The working pressures were measured using a Baratron gauge. P_w and the target voltage evolutions were monitored while varying the oxygen flow rate (q). This procedure allows following the change of the sputtering regime mode when q increases: from the elementary sputtering regime (ESR) to the compound sputtering regime (CSR). Below a critical oxygen flow rate, deposition takes place in ESR mode which generally leads to partial oxidizing conditions.[37,38] At high values of q, the sputtering regime shifts into the CSR due to the oxidation of the targets. Whatever the pressure domain (0.5, 4, and 7 Pa), we have determined that a flux of 7 sccm of oxygen was sufficient to reach equilibrated and oxidizing synthesis conditions in the chamber and the complete oxidation of the metallic elements in the deposited films.

Because the deposition rate decreases with increase in P_w, the run duration was increased for 4 and 7 Pa to reach the same thickness of 300 nm for the whole set of $NdNiO_3$ thin films. The coating thickness was determined by the step method with a Talysurf profilometer allowing an accuracy of about ±20−30 nm.

The as-deposited Nd−Ni−O thin films were X-ray amorphous, and a postannealing treatment was necessary to induce their crystallization. Soft annealing conditions under ambient air and a fairly low temperature of 820 K were carried out in a furnace during 10 h. The morphology of the films was investigated using SEM. Furthermore, the structure of the films was investigated by systematic X-ray diffraction analysis on a Brücker D8 Advance diffractometer using Cu Kα radiation. The oxygen content in the films was investigated by Rutherford backscattering spectrometry at the 3.035 MeV He^+ ion non-Rutherford cross-section resonance $^{16}O(\alpha,\alpha)^{16}O$ to improve the oxygen sensitivity. These measurements were performed at the Centro de Micro-Análisis de Materiales of Universidad Autónoma de Madrid. The spectra were processed using the SIMNRA software (more details are given in ref 39). In addition, the presence of Ni^{3+} was tracked using X-ray photoelectron spectroscopy (XPS) analysis on both as-deposited and annealed thin films. XPS measurements were carried out in a KRATOS AXIS Ultra Delay Line Detector (DLD) spectrometer using the Al Kα radiation and the constant pass energy of 1486.6 eV. The full width at half-maximum (fwhm) of the Al Kα line was lower than 0.26 eV. The photoelectron lines of the Ni^0 and Ni^{2+} $2p_{3/2}$ level of Ni and NiO powder samples were taken as references with binding energies of 852.6 and 853.3 eV, respectively.

The effect of the nickel oxidation state on the metal−insulator transition was investigated by DC electrical resistivity and IR optical transmittance measurements with a temperature ranging from liquid nitrogen (77 K) to ambient temperature. Electrical resistivity was measured in the four-point probe configuration, and a Linkam THMS600 stage was appended in the sample compartment of a Nicolet 6700 Fourier transformer infrared (FTIR) spectrometer equipped with a deuterated triglycine sulfate (DTGS) detector in the 400−7000 cm^{-1} range (i.e., 25−1.43 μm). The stage enables measurements from 77 to 870 K with an accuracy of 0.5 K.

III. RESULTS AND DISCUSSION

A. Structural Analyses. Figure 1a shows the X-ray diffractograms of 300 nm thick films annealed simultaneously

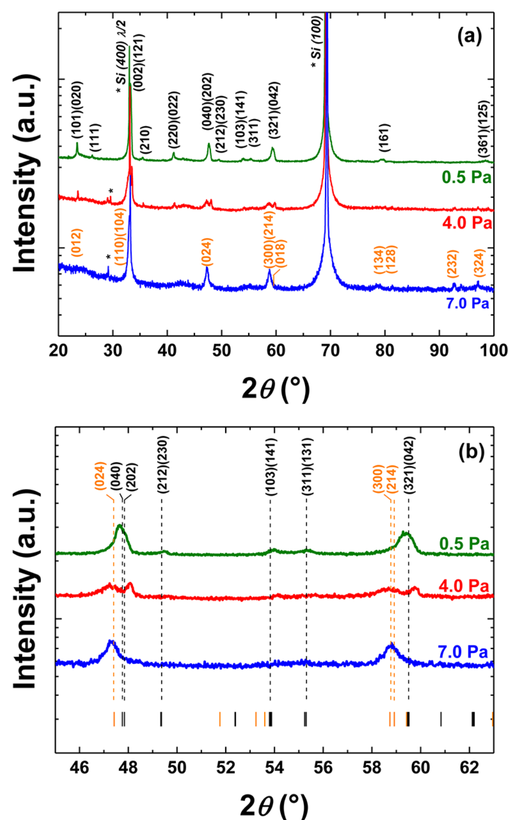

Figure 1. X-ray diffractograms of $NdNiO_{3-\delta}$ coatings deposited at 0.5, 4, and 7 Pa after air annealing at 820 K during 10 h acquired in the entire angle range (a) and an enlarged area for which the phase differentiation is well distinguished (b). The two indexations correspond to an orthorhombic cell *Pnma* space group phase (black) and a rhombohedral cell $R\bar{3}c$ space group (orange), respectively. Symbols (*) refer to the silicon substrate.

at 820 K in air, for each value of the working pressure (i.e., 0.5, 4, and 7 Pa). These diffractograms show that all samples are crystallized and that a temperature of 820 K is enough to induce crystallization of the films in the perovskite structure. Independently of P_w, the mean grain size was estimated to be close to 80 nm using the Scherrer's formula.[40]

The peaks indexed for the film deposited at 0.5 Pa correspond to the orthorhombic $GdFeO_3$-type structure, space group *Pnma* with average $a = \sqrt{2}a_p$, $b = 2a_p$, and $c = \sqrt{2}a_p$ cell parameters (where a_p is the perovskite cell parameter according to an ideal cubic cell description). A least-squares

refinement was carried out using seven instrumental parameters and four structural parameters using Topas software from Brücker. Starting lattice parameters determined by neutron diffraction were taken from ref 41. The refined parameters are a = 0.53942, b = 0.76319, and c = 0.53731 nm corresponding to a pseudocubic parameter a_p = 0.38098 nm. This value is very close to that usually observed in bulk samples (a_p = 0.3810 nm).[22] However, increasing P_w to 4 Pa, a peak splitting is evidenced for the (040) (202) and (321) (042) twin reflections of the *Pnma* phase (see Figure 1b). In perovskite structure, the peak splitting is generally due to the oxygen loss and/or the intrinsic stresses in the film. In this case, we may infer that it is caused by oxygen loss, especially since a further increase of P_w to 7 Pa leads to a rhombohedral structure. Vassiliou et al.[42] have also reported a rhombohedral $NdNiO_3$ perovskite prepared by low-temperature methods with significant oxygen deficiency. In the hexagonal description, the cell parameters of the rhombohedral phase are a = 0.54252 and c = 1.3337 nm. The Niggli-reduced cell of this sample leads to the unit cell parameters a = 0.54296 nm and α = 60.05°. The rhombohedral angle and the observed reflections close to the cubic (200) and (211) ones suggest that the material is close to becoming cubic with a superexchange angle Ni−O−Ni close to 180°.[43] This progressive phase transition vs P_w from an orthorhombic to a rhombohedral structure may be indicative of a significant oxygen deficiency in films after the annealing treatment, as investigated in the next section.

To have a better resolution on the SEM cross-section of the films, 800 nm thick films have been deposited within the same conditions. This value of thickness allows us to clearly distinguish the working pressure effect on the film morphology. Figure 2 shows the brittle-fracture cross section and surface SEM micrographs of X-ray amorphous $NdNiO_{3-\delta}$ coatings deposited on silicon substrates for the different deposition pressures P_w used.

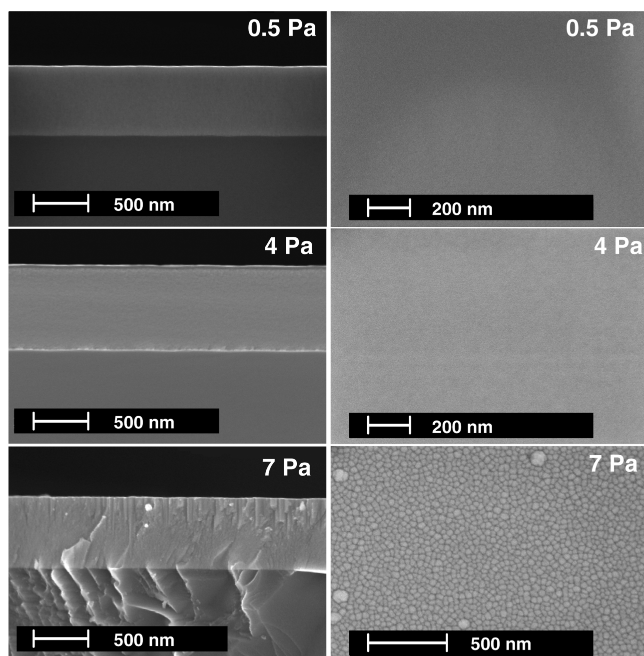

Figure 2. SEM micrographs from brittle-fracture cross-section (on the left section) and from the surface (on the right section) of 800 nm thick $NdNiO_{3-\delta}$ coatings deposited on silicon substrates at 0.5, 4, and 7 Pa without annealing.

A homogeneous dense microstructure throughout the film thickness is clearly visible at 0.5 and 4 Pa. Whereas 7 Pa becomes a drastic pressure for our suction system, a columnar microstructure takes place stepwise from the substrate. Consequently, the density of the films decreases with the pressure increase. This change with the deposition pressure is in line with a transition from zone T to zone 1 in the Thornton structure zone diagram.[44,45] The low temperature during the film growth (∼370 K), associated with less drastic bombardment conditions (O^- ions and Ar^0 neutrals essentially), promotes the development of a columnar structure, usually associated to the development of gaps between the columns. This structure evolution is well confirmed by the SEM observations of the film surface (Figure 3). Indeed, at 0.5 and 4 Pa, an unvarying smooth surface confirms the transverse section investigations. Unlike this kind of microstructure, the film deposited at 7 Pa presents a significant roughness. A cauliflower-like morphology leads to open-structured films with a column width distribution to be close to 50 nm.

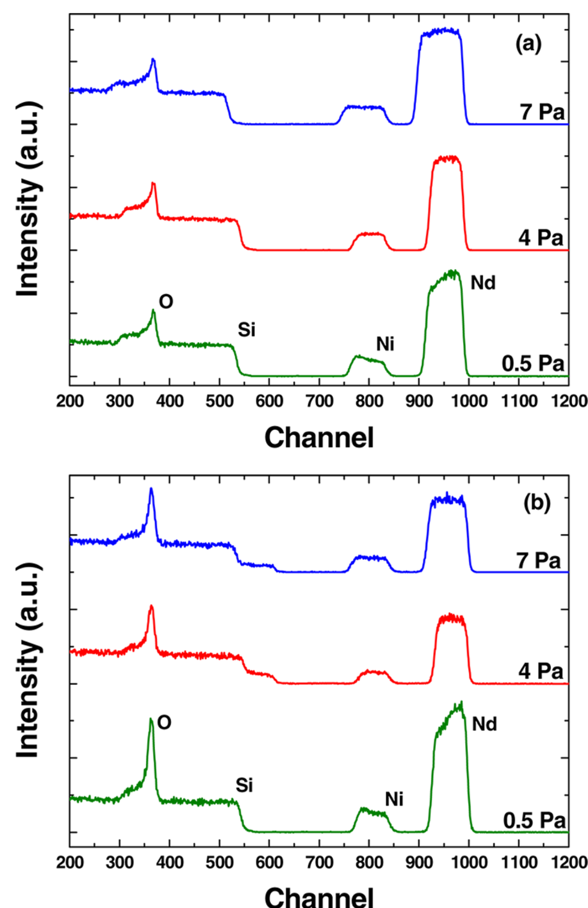

Figure 3. RBS spectra of the $NdNiO_{3-\delta}$ as-deposited films (a) and films annealed at 820 K (b).

B. Oxygen Deficiency in the Films. To investigate the oxygen content in our films, RBS measurements were performed. SIMNRA simulations were carried out assuming a single $NdNiO_{3-\delta}$ layer on the silicon substrate for 4 and 7 Pa (see Figure 3). A simulation based on a multilayer $NdNiO_3$ approach was necessary to take into account fluctuations in the

chemical composition of the film deposited at 0.5 Pa. Moreover, a very precise fitting was obtained with an interfacial SiO_2 layer of about 10−20 nm thickness between the $NdNiO_{3-\delta}$ film and the silicon substrate. The plateau located below channel 600 for the 4 and 7 Pa annealed films can be modeled considering a partial delamination of the films leaving part of the silicon surface uncovered (Figure 3b). Figure 4 and Table 1 indicate the value of the oxygen deficiency parameter δ in as-deposited and annealed films for each pressure.

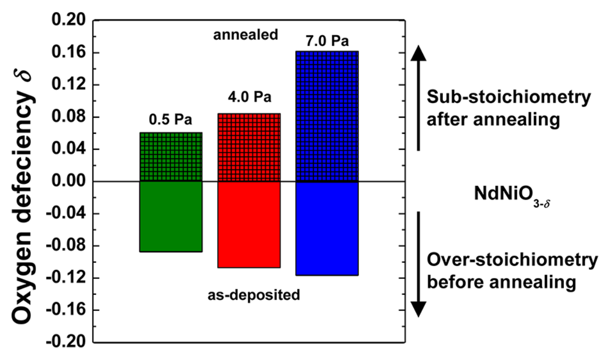

Figure 4. Oxygen deficiency measured by RBS in $NdNiO_{3-\delta}$ in as-deposited films and in films annealed at 820 K for deposition pressure of 0.5, 4, and 7 Pa.

Table 1. Results of the RBS Simulations Using SIMNRA from the RBS Data Acquired on the $NdNiO_{3-\delta}$ As-Deposited and Annealed Films for Different Deposition Pressures

		Nd (at. %)	Ni (at. %)	O (at. %)	δ
0.5 Pa	as-deposited	21.0	18.0	60.7	−0.087
	annealed	21.5	19.0	59.5	0.061
4 Pa	as-deposited	21.3	16.8	62.9	−0.107
	annealed	22.8	17.8	59.3	0.084
7 Pa	as-deposited	18.9	16.4	63.4	−0.117
	annealed	21.6	19.6	58.7	0.162

The results reveal that the Nd/Ni atomic ratio is close to 1.15 in films deposited at 0.5 and 7 Pa and is close to 1.25 in the film deposited at 4 Pa. However, small changes in this ratio do not seem to affect the physical properties of the films. For the sake of simplicity we use the δ parameter to evaluate the deviation of the oxygen content from the $NdNiO_3$ stoichiometry in crystalline and X-ray amorphous films. The δ parameter appears as negative within the entire set of as-deposited films, suggesting a full oxidation of the metallic elements in Ni^{3+} and Nd^{3+} before annealing. This can be explained by the deposition of the coatings in the compound sputtering regime. However, δ becomes positive after annealing in air at 820 K. After annealing, the oxygen deficiency of the 0.5 Pa film is $\delta = 0.061$ (i.e., $NdNiO_{2.94}$). Indeed, the reduction of the Ni^{3+} ion is fairly limited, and the postannealed film still adopts the orthorhombic symmetry as shown by the X-ray analysis. As the oxygen content is sufficient, this structure is still observed. Increasing the pressure to 4 Pa, the oxygen deficiency rises to $\delta = 0.084$ (i.e., $NdNiO_{2.92}$), and the $R\bar{3}c$ rhombohedral symmetry appears. At 7 Pa, the oxygen loss is much more pronounced ($\delta = 0.162$) and explains the shifting of the *Pnma* orthorhombic symmetry at low P_w toward a pure $R\bar{3}c$ rhombohedral one at high P_w. The increase of the oxygen loss is likely explained by the microstructural feature that promotes the exchange and diffusion of oxygen outside the opened surface of the film. Indeed, oxygen diffusion is very sensitive to columnar structure and film density, as observed at 7 Pa which could take part in oxygen channeling and promote oxygen loss. Such a microstructural effect was also observed in based nickel spinel sintered at different temperatures by Jung et al.[46] The appearance of porosity affects the oxidation and reduction of the material during the thermal treatment and can be related to the oxygen exchanges with the surrounding medium. This work is consistent with the oxygen departure in based nickel oxide ceramics during the thermal treatment according to the microstructure.

As the stabilization of the Ni^{3+} ion plays a decisive role in suitable thermochromic $NdNiO_3$ coatings, it is important to assess the Ni^{3+} content evolution in our films throughout the experimental process. Since XPS was successfully used to check the Ni^{3+} ion disproportionation effect in the $ReNiO_3$ elpasolite structure below the MIT,[47,48] the RBS measurements have been complemented by photoemission analyses. To discriminate pressure and thermal treatment effects, XPS analyses were systematically implemented on as-deposited and annealed films. The Nd 3d, Ni 2p, and O 1s core-level spectra were observed in the entire XPS spectra for all $NdNiO_{3-\delta}$ films. First, we focus on the Ni $2p_{3/2}$ level that allows differentiating the ionization states of nickel (Figure 5).

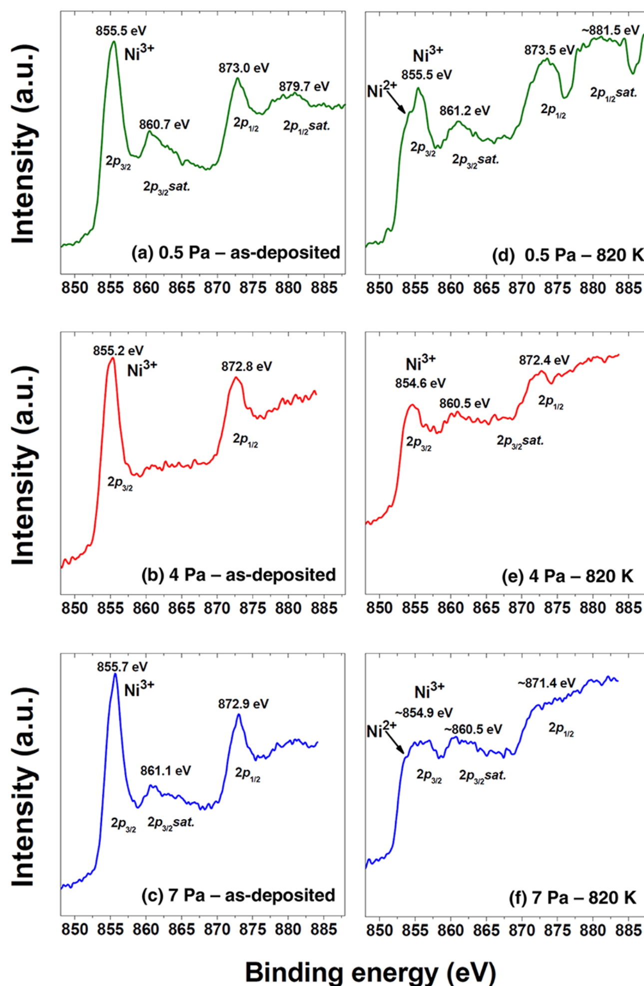

Figure 5. Photoelectron spectra of Ni $2p_{3/2}$ and $2p_{1/2}$ levels taken in as-deposited films for 0.5 Pa (a), 4 Pa (b), and 7 Pa (c) and annealed films for 0.5 Pa (d), 4 Pa (e), and 7 Pa (f).

dx.doi.org/10.1021/jp4111597 | J. Phys. Chem. C 2014, 118, 5908−5917

The corresponding core-level spectra of all the as-deposited films exhibit a peak well localized at a binding energy ranging from 855.2 to 855.7 eV, which is assigned to trivalent nickel.[47−50] The same conclusion is drawn from the signal at the Ni $2p_{1/2}$ level. These results interestingly reveal that Ni^{3+} is stabilized during the deposition step independently of the deposition pressure. The signal localized around 860.5 eV is associated to a satellite peak due to the charge-transfer multielectron excitation.[51]

In the case of the annealed films, a characteristic depletion of the Ni^{3+} $2p_{3/2}$ (around 855 eV) photoelectron line intensity appears driven by the trivalent Ni destabilization. Considering the different working pressures, the lower intensity of the peak means the Ni^{3+} content tends to decrease more markedly when the pressure increases. This result is in good agreement with RBS measurements and can again be related to the oxygen loss due to the opened microstructure. Note that the shoulder of Ni^{2+} localized at a binding energy of 853.3 eV does not appear as clearly as in Nd_2NiO_4 and NiO, which tends to confirm the absence of these phases as suggested from the XRD analyses. Unfortunately, the quantification of the Ni^{2+}/Ni^{3+} ionic ratio is difficult for two main reasons. First, delamination occurring during the heat treatment degrades the quality of the signal which becomes noisy after annealing. Furthermore, additional satellite peaks of the Ni^{2+} $2p_{3/2}$ level (around 856.3 and 861.7 eV) overlap peaks of Ni^{3+} (around 855.5 and 860.5 eV) and make it extremely difficult to deconvolute the Ni^{2+} satellite peaks with accuracy.

The excess oxygen measured by RBS on X-ray amorphous films can be related to an overoxidation of the material or the insertion of molecular oxygen in the film during the sputtering process. From an energetical point of view, it is more difficult to stabilize Ni^{4+} than Nd^{4+} (4th ionization energy is equal to 54.9 eV against 40.4 eV, respectively[21]). Considering the case of overoxidation, which could occur during the deposition process by the formation of the Nd^{4+}, the Nd $3d_{5/2}$ and $3d_{3/2}$ core-level spectra of the as-deposited films were investigated in detail (Figure 6).

The presence of an Auger peak from the KLL level of oxygen partially overlaps the $3d_{5/2}$ peak of Nd. Nevertheless, the characteristic line of the Nd $3d_{5/2}$ can be estimated around 981.7 eV. This result is close to the value reported by Sarma et al.[52] at 982.0 eV in Nd_2O_3. This signal can be easily assigned to the Nd^{3+} state. In addition, the detection limit of the XPS measurements is close to 0.1 at. %, and the presence of the Nd^{4+} state should appear as a shoulder feature around 983 eV. The absence of such a signal on both $3d_{5/2}$ and $3d_{3/2}$ levels advocates the incorporation of oxygen excess in molecular form instead of the formation of Nd^{4+}. Molecular oxygen incorporation into the film during the deposition process has been evidenced by others in thin ZnO films deposited in reactive mode under oxygen-rich deposition conditions.[53,54] Moreover, the position of the Nd $3d_{5/2}$ level is shifted from 981.3 to 981.5 and 982.2 eV for 0.5, 4, and 7 Pa, respectively, owing to the improvement of the oxidation of Nd in Nd^{3+} with the oxygen partial pressure. Increasing the working pressure in the deposition chamber has two associated opposite effects. First, the incorporation of additional oxygen into the film could be enhanced by the increase in oxygen partial pressure. However, the collision rate of the sputter species through the plasma increases with the total pressure P_w.[55−57] As a consequence, the species are more easily thermalized at higher deposition pressures, and the average energy available per adatom on the sample surface is not sufficient to produce dense layers by transfer of the momentum. To have an overview of this energetic consideration, there is a need to differentiate in the collisional approach the average kinetic energies of the sputter metallic species (Ni and Nd) and the accelerated O^- ions tracing to the direct desorption of O^- from the target[58] or the combination of atomic oxygen with an electron near the target, as well as neutral Ar^0 atoms reflected on the target toward the films.[59,60] The average kinetic energy of the O^- is close to the bias voltage (i.e., 100−200 eV), while the Ar^0 one is smaller (i.e., 10−30 eV) at 0.5 Pa.[61] It should be noted that the fastest O^- ions impinging the surface of the film during the growth may be implanted as additional oxygen over a few nanometers of depth of the film.[54] The average kinetic energy of the sputter species is much lower (typically by 2 orders of magnitude) than the O^- one.[60,62,63] Bearing in mind that the kinetic energy decreases swiftly with P_w, O^- ions and Ar^0 neutrals may play a fundamental role in the densification of the films at lower pressures but cannot explain by itself the stabilization of Ni^{3+} whatever P_w confirmed by XPS. Therefore, we propose that the simultaneous cosputtering of neodymium stabilizes Ni^{3+} in an X-ray amorphous $NdNiO_{3-\delta}$ thin film. In the perovskite family, various 3d transition metals are stabilized in usually high oxidation states that cannot be accessed in binary compounds with oxygen.[64] The Ni^{3+} uncommon oxidation state is stabilized through the covalent Ni−O interactions that arise when a highly electropositive counter-cation such as Nd is present to drive electron donation from oxygen to the more electronegative transition metal by an inductive effect well-known in organic and solid-state chemistry.[65,66] The electropositive Nd cation (electronegativity of 1.14 in Pauling scale[21]) promotes increased orbital overlap between oxygen and the electronegative Ni cation (electronegativity of 1.91[21]) by destabilizing the O2p states. Electrostatic interactions occurring between cations and oxygen most likely foreshadow the existence of a local order and the presence of Ni^{3+} in a NiO_6 octahedral configuration.

However, solid-state reactions based on the NiO and Nd_2O_3 metal oxide powder mixtures under near ambient conditions lead to only partially stabilized perovskites.[19,20,42,43,67,12,68] Therefore, we assume that the deposition process also participates in the stabilization of the high oxidation state of

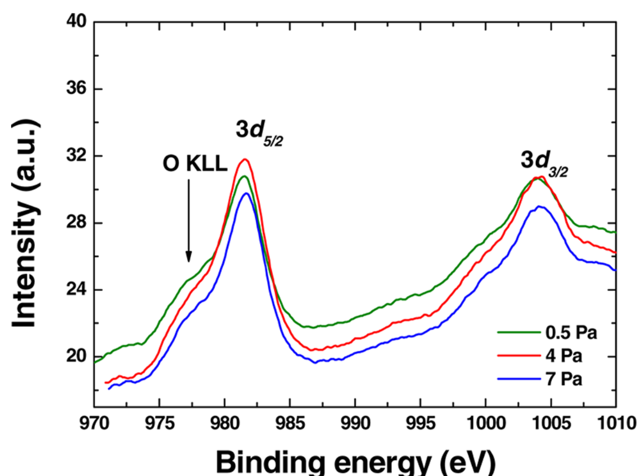

Figure 6. Photoelectron spectra of Nd $3d_{5/2}$ and $3d_{3/2}$ levels taken on as-deposited films for 0.5, 4, and 7 Pa.

Ni. The specificity of the sputtering process is to generate high cooling rates, up to 10^{13} K/s,[69] of the sputtered species during their condensation over the substrate, which is similar to a tempering process that nearly "freezes" the local configuration of atoms adsorbing to the substrate.

The combination of the inductive effect and the rapid condensation of the species over the substrate in non-equilibrium thermodynamic conditions may explain the stabilization of metastable X-ray amorphous $NdNiO_{3-\delta}$ films.

These results suggest that plasma properties and the mechanisms involved during the deposition step explain that the $NdNiO_{3-\delta}$ phase is obtained despite the less drastic annealing conditions than those generally used. The post-annealing step is performed only to crystallize the material and not to oxidize Ni^{2+} into Ni^{3+} as usually described in the literature.

C. Electronic Transport Properties. To have an overview of the influence of oxygen deficiency on the electronic transport properties, the DC electrical resistivity was investigated using the four-point probe method varying the temperature from liquid nitrogen to room temperature as shown in Figure 7.

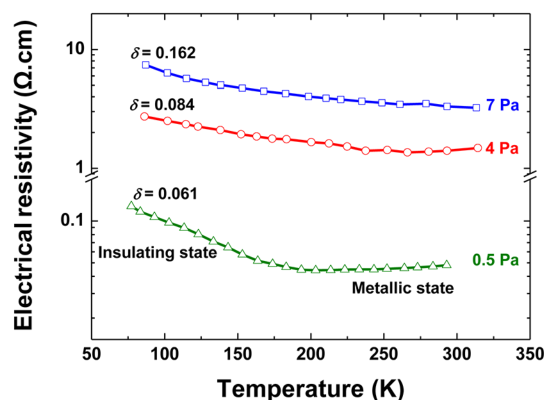

Figure 7. Evolution of DC electrical resistivity versus temperature for the films deposited at 0.5, 4, and 7 Pa and annealed under atmospheric conditions at 820 K.

The variation of the working pressure strongly affects the electrical properties of the $NdNiO_{3-\delta}$ coatings. A sharp electrical transition is observed only for the coating deposited at 0.5 Pa and corresponds to an oxygen deficiency $\delta = 0.061$. A jump of half order of magnitude is reached between the high-temperature metallic state and low-temperature insulating state without the presence of the hysteresis phenomenon. The electrical jump becomes negligible for the samples deposited at 4 and 7 Pa that exhibit higher oxygen losses, i.e., $\delta > 0.084$. In the high-temperature range, the metallic behavior of the films deposited at 4 Pa is hardly evidenced, while it vanishes at 7 Pa. A slight deviation δ in oxygen stoichiometry of the network $NdNiO_{3-\delta}$ has a substantial effect on the electronic transport properties of the system. For example, in TiO_{2-x}[70] or CeO_{2-x}[71] substoichiometric oxides, oxygen vacancies induce a charge effect on cation sites which reduces the mobility by a strong electron−lattice coupling in the model of the small polarons. Banerjee et al.[72] and Pi et al.[73] both have observed a polaron hopping conduction in rare earth manganites, and Blasco et al.[74] were provided evidence of an electron trapping by a polaronic effect in $NdNiO_{3-\delta}$. Thus, there is a strong correlation between structural and electrical transport properties in this system which can be explained by a polaronic state. When δ increases, the strength of the electron−phonon coupling increases which results in localization of charge carriers. On that account, the modification of the polaronic state with oxygen departure probably must be considered as the main effect on the resistivity. Nevertheless, the hypothesis of the microstructure effect on the electronic transport cannot be entirely excluded. Indeed, the critical oxygen deficiency to deteriorate the MIT is estimated close to 0.084 and is less important than values which have been reported elsewhere. Nikulin et al.[20] have observed a drastic blurring of the metal−insulator contrast for oxygen deficiencies for $\delta > 0.2$ in $NdNiO_{3-\delta}$ ceramics elaborated using the nitric method. Beyond $\delta = 0.2$, the electrical contrast exhibits an unsharpened transition. Even so, in the mentioned study, all samples show a similar microstructure regardless of the oxygen content. In our case, we assume that the decrease of the critical oxygen deficiency can also be attributed to the porous microstructure of the films. It should be emphasized that the porosities and microcracks, as well as the small grain size, appearing during the crystallization should be acting as local transport barriers of the electronic carriers increasing the overall resistivity of the films. Thus, the columnar structure is suggested to account for both an increase in the overall electrical resistivity for the sample deposited at 7 Pa and a decrease in the critical oxygen deficiency combined with a blurred metal−insulator transition.

Nevertheless, the effect of the oxygen content on the electronic transport behavior described above must be uncoupled from the orthorhombic−rhombohedral phase transition driven by the decrease in the oxygen stoichiometry in the structure. The well-established Zaanen−Sawatski−Allen (ZSA) model is widely accepted to describe the electronic conduction mechanisms in perovskites.[12,75] The structural alteration induced by the oxygen loss may be explained within the ZSA approach by a straightening of the Ni−O−Ni bond angle that stabilizes the metallic state over the semiconducting state, so lowering the MIT temperature. Therefore, an overlap occurs between the Ni_{3d} and O_{2p} states that promotes the charge transfer leading to enhanced metallicity.[76] Above the MIT, $NdNiO_{3-\delta}$ adopts the orthorhombic structure with a *Pnma* space group. In this symmetry, the Ni−O−Ni superexchange angle is close to 157.16° at room temperature.[41,77] As a consequence, the fully O_{2p} band partially overlaps the filled Ni_{3d} conduction band, and DC metallic electrical conduction is achieved. On the contrary, decreasing the temperature below the MIT induces a phase transition to a monoclinic structure of $P2_1/n$ space group and the enclosure of the Ni−O−Ni superexchange angle around 156.17° at 100 K. Consequently, an electrical band gap appears between the valence bands of nickel and oxygen. In these conditions, the perovskite shows a semiconducting behavior. The superexchange angle of the unwanted rhombohedral $NdNiO_{3-\delta}$ phase is close to that of $LaNiO_3$ (165.21° at room temperature[41]) that owns the same structure and exhibits a pure metallic behavior over the whole temperature range. This structural feature may be accounted for by an enhanced metallicity stabilized toward the lower-temperature range. According to the ZSA theory, the rhombohedral sample deposited at 7 Pa should be metallic. The stabilization of the metallic behavior is not evidenced in this case suggesting that oxygen vacancies play a more prominent role in the electronic properties than the structural transition.

D. Infrared Properties. The IR optical transmittance spectra from 90 to 290 K confirm structural and electrical

results. An interesting optical switching from a transparent state at low temperature to an opaque state in the metallic domain is observed only for the sample deposited at a working pressure of 0.5 Pa and annealed (Figure 8). The metal−insulator transition

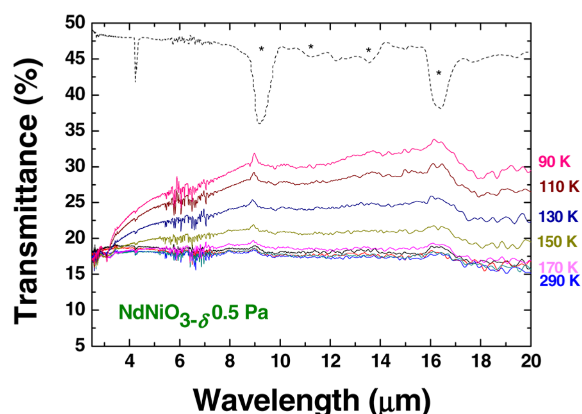

Figure 8. Infrared transmittance spectra from 90 to 290 K of an annealed $NdNiO_{3-\delta}$ thin film of 300 nm thickness deposited at 0.5 Pa. The dashed line reports the native SiO_2/Si spectrum and its different absorption bands (*).

is estimated close to 170 K. The indexed absorption bands at 9.1, 12.3, 13.4, and 16.4 μm are assigned to the native layer of SiO_2 (bands designed by stars in Figure 8). The discernible band at 17.5 μm for lower temperatures corresponds to the stretching of the Ni−O bond in NiO_6 octahedrons.[78]

To quantify the optical features versus the synthesis pressure in the different transparency bands of the atmosphere, the average intensity $1/(\Delta\lambda)\int I(\lambda)/I_0 d\lambda$ was computed for each temperature. The curves are plotted in Figure 9 for the

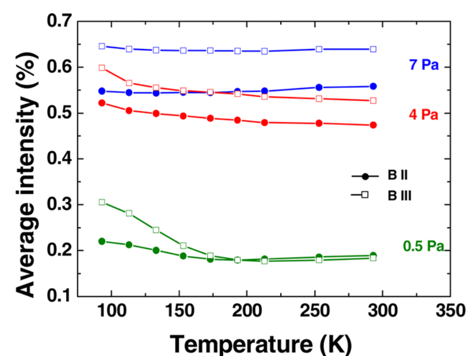

Figure 9. Average intensity versus temperature computed from infrared spectra in bands II and III for $NdNiO_{3-\delta}$ coatings deposited at 0.5, 4, and 7 Pa.

transparency bands II (3−5 μm) and III (8−12 μm). It is useful to define the optical contrast factor as $\tau(\lambda) = (\tau_{LT} - \tau_{HT})$ where τ_{LT} and τ_{HT} are the transmittance at low and high temperatures, respectively, and λ is the IR wavelength. A band contrast factor $\tau(\Delta\lambda)$ for the spectral band $\Delta(\lambda)$ II and III characterizing the IR optical transmission switching efficiency can also be defined.

The band contrast factor reaches 3% and 12% in band II and band III, respectively, whereas this one becomes negligible increasing the pressure: 1% (BII) and 5% (BIII) for 4 Pa and less than 1% (BII and BIII) for 7 Pa. The working pressure affects widely the optical contrast mainly through the structure and oxygen content of the films. The optical contrast is observed as long as the orthorhombic phase is stabilized. The best optical contrast is observed for the film deposited at 0.5 Pa. The transmittance increases according to the resistivity increase for the rhombohedral phase.

IV. CONCLUSIONS

The effect of the deposition pressure was investigated on the chemical, structural, electrical, and IR optical properties of $NdNiO_{3-\delta}$ thin films elaborated by the reactive magnetron cosputtering process. Whatever the deposition pressure, RBS and XPS measurements clearly evidenced that the Ni^{3+} oxidation state is achieved thanks to the DC magnetron sputtering process in the compound sputtering regime. Although an oxygen loss is observed during the subsequent soft annealing, the first step of the process allows inducing the crystallization of the thermochromic phase. The condition to reach the thermochromic phase is to grow a dense thin film at low deposition pressure such as 0.5 Pa with a relatively low target−substrate distance. Despite that the oxygen overstoichoimetry is enhanced in as-deposited films due to the oxygen partial pressure increase with the total deposition pressure, the latter parameter promotes oxygen loss during the annealing step. Increasing the deposition pressure generates porous thin films, which was proposed to promote the reduction of Ni^{3+} in Ni^{2+} owing to the diffusion of oxygen through surface exchange with the surrounding medium. As a consequence, a structural transition from the thermochromic orthorhombic phase to a nonthermochromic rhombohedral phase was evidenced. This work was necessary to elucidate the mechanisms of oxidation in $NdNiO_{3-\delta}$ thermochromic thin films synthesized by reactive DC sputtering followed by a soft annealing in air. This work may be extended to other $ReNiO_3$ thin films to reduce their annealing temperature and oxygen pressure while keeping the jump of the MIT. These results represent a significant improvement in the vulgarization of thermochromic nickelates and the possibility to work on a large substrate scale using a high deposition rate.

■ AUTHOR INFORMATION

Corresponding Author

*E-mail: fabien.capon@univ-lorraine.fr. Phone: +33 (0) 83 58 42 52.

Notes

The authors declare no competing financial interest.

■ ACKNOWLEDGMENTS

The authors acknowledge A. Renard (LCPME) for the XPS analyses of as-deposited and annealed films.

■ REFERENCES

(1) Christmann, T.; Felde, B.; Niessner, W.; Schalch, D.; Scharmann, A. Thermochromic VO_2 Thin Films Studied by Photoelectron Spectroscopy. *Thin Solid Films* **1996**, *287*, 134−138.

(2) Beteille, F.; Livage, J. Optical Switching in VO_2 Thin Films. *J. Sol-Gel Sci. Technol.* **1998**, *13*, 915−921.

(3) Saitzek, S.; Guinneton, F.; Guirleo, G.; Sauques, L.; Aguir, K.; Gavarri, J.-R. VO_2 Thin Films Deposited on Silicon Substrates from V_2O_5 Target: Limits in Optical Switching Properties and Modeling. *Thin Solid Films* **2008**, *516*, 891−897.

(4) Wittlin, A.; Gerrits, A. M.; Granados, X.; Garcia-Munoz, J. L.; Fontcuberta, J. Far-Infrared Studies of the Metal-Insulator Transition in $PrNiO_3$ and $NdNiO_3$. *Phys. C Supercond.* **1994**, *235*, 1289−1290.

(5) DeNatale, J. F.; Kobrin, P. H. Optical Switching in Thin Film $NdNiO_3$. *MRS Proc.* **2012**, *479*.

(6) Laffez, P.; Zaghrioui, M.; Reversat, L.; Ruello, P. Electron Doped $(Sm_{1-x},Ca_x)MnO_3$ Perovskite Manganite as Potential Infrared Thermochromic Switch. *Appl. Phys. Lett.* **2006**, *89*, 081909.

(7) Boileau, A.; Capon, F.; Barrat, S.; Laffez, P.; Pierson, J. F. Thermochromic Effect at Room Temperature of $Sm_{0.5}Ca_{0.5}MnO_3$ Thin Films. *J. Appl. Phys.* **2012**, *111*, 113517.

(8) Capon, F.; Boileau, A.; Carteret, C.; Martin, N.; Boulet, P.; Pierson, J. F. Cation Size Effect on the Thermochromic Properties of Rare Earth Cobaltites $RECoO_3$ (RE: La, Nd, Sm). *J. Appl. Phys.* **2013**, *114*, 113510.

(9) Capon, F.; Laffez, P.; Bardeau, J.-F.; Simon, P.; Lacorre, P.; Zaghrioui, M. Metal−insulator Transition at Room Temperature and Infrared Properties of $Nd_{0.7}Eu_{0.3}NiO_3$ Thin Films. *Appl. Phys. Lett.* **2002**, *81*, 619.

(10) Ambrosini, A.; Hamet, J.-F. $Sm_xNd_{1-x}NiO_3$ Thin-Film Solid Solutions with Tunable Metal−insulator Transition Synthesized by Alternate-Target Pulsed-Laser Deposition. *Appl. Phys. Lett.* **2003**, *82*, 727.

(11) Capon, F.; Ruello, P.; Bardeau, J.-F.; Simon, P.; Laffez, P.; Dkhil, B.; Reversat, L.; Galicka, K.; Ratuszna, A. Metal−insulator Transition in Thin Films of R_xR_{1-x}' NiO_3 Compounds: DC Electrical Conductivity and IR Spectroscopy Measurements. *J. Phys.: Condens. Matter* **2005**, *17*, 1137−1150.

(12) Lacorre, P.; Torrance, J. B.; Pannetier, J.; Nazzal, A. I.; Wang, P. W.; Huang, T. C. Synthesis, Crystal Structure, and Properties of Metallic $PrNiO_3$: Comparison with Metallic $NdNiO_3$ and Semiconducting $SmNiO_3$. *J. Solid State Chem.* **1991**, *91*, 225−237.

(13) Griffiths, C. H. Influence of Stoichiometry on the Metal-Semiconductor Transition in Vanadium Dioxide. *J. Appl. Phys.* **1974**, *45*, 2201.

(14) Bowman, R. M.; Gregg, J. M. VO_2 Thin Films: Growth and the Effect of Applied Strain on Their Resistance. *J. Mater. Sci.: Mater. Electron.* **1998**, *9*, 187−191.

(15) Xu, S.; Ma, H.; Dai, S.; Jiang, Z. Study on Optical and Electrical Switching Properties and Phase Transition Mechanism of Mo^{6+}-Doped Vanadium Dioxide Thin Films. *J. Mater. Sci.* **2004**, *39*, 489−493.

(16) Youn, D.-H. Growth Optimization and Electrical Characteristics of VO_2 Films on Amorphous SiO_2/Si Substrates. *J. Appl. Phys.* **2004**, *95*, 1407.

(17) Zhen-Fei, L.; Zhi-Ming, W.; Xiang-Dong, X.; Tao, W.; Ya-Dong, J. Study of Nanocrystalline VO_2 Thin Films Prepared by Magnetron Sputtering and Post-Oxidation. *Chin. Phys. B* **2010**, *19*, 106103.

(18) Laffez, P.; Ruello, P.; Edely, M. Electrical and Infrared Properties of RF Sputtering Rare Earth Nickelate ($RNiO_3$) Thin Films with Metal-Insulator Transtion. *Leading-Edge Mater. Sci. Res.* **2008**, 277.

(19) Tiwari, A.; Rajeev, K. P. Effect of Oxygen Stoichiometry on the Electrical Resistivity Behaviour of $NdNiO_{3-\delta}$. *Solid State Commun.* **1998**, *109*, 119−124.

(20) Nikulin, I. V.; Novojilov, M. A.; Kaul, A. R.; Mudretsova, S. N.; Kondrashov, S. V. Oxygen Nonstoichiometry of $NdNiO_{3-\delta}$ and $SmNiO_{3-\delta}$. *Mater. Res. Bull.* **2004**, *39*, 775−791.

(21) Lide, D. R. *CRC Handbook of Chemistry and Physics: A Ready-Reference Book of Chemical and Physical Data: 2006−2007*; CRC Press: Boca Raton, 2006.

(22) Medarde, M. L. Structural, Magnetic and Electronic Properties of Perovskites (R= Rare Earth). *J. Phys.: Condens. Matter* **1997**, *9*, 1679.

(23) *The Condensed Chemical Dictionary*, 10th ed.; rev. by Gessner G. Hawley; Van Nostrand Reinhold Co: New York, 1981.

(24) Napierala, C.; Edely, M.; Laffez, P.; Sauques, L. Thermo-Optical Effect of $Nd_{0.3}Sm_{0.7}NiO_3$ Ceramic in the Infrared Range. *Opt. Mater.* **2009**, *31*, 1498−1501.

(25) DeNatale, J. F.; Kobrin, P. H. Lattice Distortion Effects on Electrical Switching in Epitaxial Thin Film $NdNiO_3$. *J. Mater. Res.* **2011**, *10*, 2992−2995.

(26) Escote, M. T.; Jardim, R. F. Structural and Transport Properties of $NdNiO_3$ Thin Films Made by RF Sputtering. *J. Magn. Magn. Mater.* **2001**, *226−230*, 249−251.

(27) Laffez, P.; Retoux, R.; Boullay, P.; Zaghrioui, M.; Lacorre, P.; van Tendeloo, G. Transmission Electron Microscopy of $NdNiO_3$ Thin Films on Silicon Substrates. *Eur. Phys. J. Appl. Phys.* **2000**, *12*, 55−60.

(28) Laffez, P.; Zaghrioui, M.; Retoux, R.; Lacorre, P. Oriented and Polycrystalline $NdNiO_3$ Thin Films on Silicon Substrate. *J. Magn. Magn. Mater.* **2000**, *211*, 111−117.

(29) Novojilov, M. A.; Gorbenko, O. Y.; Graboy, I. E.; Kaul, A. R.; Zandbergen, H. W.; Babushkina, N. A.; Belova, L. M. Perovskite Rare-Earth Nickelates in the Thin-Film Epitaxial State. *Appl. Phys. Lett.* **2000**, *76*, 2041.

(30) Gorbenko, O. Y.; Novojilov, M. A.; Graboy, I. E.; Amelichev, V. A.; Bosak, A. A.; Nikulin, I. V.; Kaul, A. R.; Guettler, B.; Wahl, G.; Babushkina, N. A. Lattice Strain in the Epitaxial Thin Films of Perovskites. *Int. J. Inorg. Mater.* **2001**, *3*, 1303−1305.

(31) Catalan, G.; Bowman, R. M.; Gregg, J. M. Metal-Insulator Transitions in $NdNiO_3$ Thin Films. *Phys. Rev. B* **2000**, *62*, 7892.

(32) Kaur, D.; Jesudasan, J.; Raychaudhuri, P. Pulsed Laser Deposition of $NdNiO_3$ Thin Films. *Solid State Commun.* **2005**, *136*, 369−374.

(33) Napierala, C.; Lepoittevin, C.; Edely, M.; Sauques, L.; Giovanelli, F.; Laffez, P.; VanTedeloo, G. Moderate Pressure Synthesis of Rare Earth Nickelate with Metal−insulator Transition Using Polymeric Precursors. *J. Solid State Chem.* **2010**, *183*, 1663−1669.

(34) Capon, F.; Horwat, D.; Pierson, J. F.; Zaghrioui, M.; Laffez, P. Thermochromic Effect in $NdNiO_{3-\delta}$ Thin Films Annealed in Ambient Air. *J. Phys. D: Appl. Phys.* **2009**, *42*, 182006.

(35) Capon, F.; Horwat, D.; Pierson, J. F.; Chapusot, V.; Billard, A. Strontium-Doped Lanthanum Manganite Coatings Crystallised after Air Annealing of Amorphous Co-Sputtered Films. *Mater. Chem. Phys.* **2009**, *116*, 219−222.

(36) Tranvouez, N.; Pierson, J. F.; Capon, F.; Bauer, P. Effect of the Deposition Process on the Composition and Structure of Sputtered Lanthanum Cuprate Films. *Surf. Coat. Technol.* **2011**, *205*, S254−S257.

(37) Safi, I. Recent Aspects Concerning DC Reactive Magnetron Sputtering of Thin Films: A Review. *Surf. Coat. Technol.* **2000**, *127*, 203−218.

(38) Depla, D.; Buyle, G.; Haemers, J.; De Gryse, R. Discharge Voltage Measurements during Magnetron Sputtering. *Surf. Coat. Technol.* **2006**, *200*, 4329−4338.

(39) Mayer, M. *SIMNRA User's Guide*; Max-Planck-Institut für Plasmaphysik: Germany, 1997.

(40) Klug, H. P. *X-Ray Diffraction Procedures for Polycrystalline and Amorphous Materials*, 2nd ed.; Wiley: New York, 1974.

(41) Garcia-Munoz, J. L.; Rodriguez-Carvajal, J.; Lacorre, P.; Torrance, J. B. Neutron-Diffraction Study of $RNiO_3$ (R= La, Pr, Nd, Sm): Electronically Induced Structural Changes across the Metal-Insulator Transition. *Phys. Rev. B* **1992**, *46*, 4414.

(42) Vassiliou, J. K.; Hornbostel, M.; Ziebarth, R.; Disalvo, F. J. Synthesis and Properties of $NdNiO_3$ Prepared by Low-Temperature Methods. *J. Solid State Chem.* **1989**, *81*, 208−216.

(43) Mahesh, R.; Kannan, K. R.; Rao, C. N. R. Electrochemical Synthesis of Ferromagnetic $LaMnO_3$ and Metallic $NdNiO_3$. *J. Solid State Chem.* **1995**, *114*, 294−296.

(44) Thornton, J. A. Influence of Apparatus Geometry and Deposition Conditions on the Structure and Topography of Thick Sputtered Coatings. *J. Vac. Sci. Technol.* **1974**, *11*, 666.

(45) Thornton, J. A. High Rate Thick Film Growth. *Annu. Rev. Mater. Sci.* **1977**, *7*, 239−260.

(46) Jung, J.; Töpfer, J.; Mürbe, J.; Feltz, A. Microstructure and Phase Development in $NiMn_2O_4$ Spinel Ceramics during Isothermal Sintering. *J. Eur. Ceram. Soc.* **1990**, *6*, 351−359.

(47) Galicka, K.; Szade, J.; Ruello, P.; Laffez, P.; Ratuszna, A. The Photoemission Study of $NdNiO_3/NdGaO_3$ Thin Films, through the Metal−insulator Transition. *Appl. Surf. Sci.* **2009**, *255*, 4355−4361.

(48) Bilewska, K.; Wolna, E.; Edely, M.; Ruello, P.; Szade, J. Evidence of Charge Disproportionation on the Nickel Sublattice in $EuNiO_3$ Thin Films: X-Ray Photoemission Studies. *Phys. Rev. B* **2010**, *82*.

(49) Aydogdu, G. H.; Ha, S. D.; Viswanath, B.; Ramanathan, S. Epitaxy, Strain, and Composition Effects on Metal-Insulator Transition Characteristics of $SmNiO_3$ Thin Films. *J. Appl. Phys.* **2011**, *109*, 124110.

(50) Chien, F. S.-S.; Wu, Y. T.; Lai, G. L.; Lai, Y. H. Disproportionation and Comproportionation Reactions of Resistive Switching in Polycrystalline NiO_x Films. *Appl. Phys. Lett.* **2011**, *98*, 153513.

(51) Kim, K. S.; Baitinger, W. E.; Amy, J. W.; Winograd, N. ESCA Studies of Metal-Oxygen Surfaces Using Argon and Oxygen Ion-Bombardment. *J. Electron Spectrosc. Relat. Phenom.* **1974**, *5*, 351−367.

(52) Sarma, D. D.; Rao, C. N. R. XPES Studies of Oxides of Second- and Third-Row Transition Metals Including Rare Earths. *J. Electron Spectrosc. Relat. Phenom.* **1980**, *20*, 25−45.

(53) Yuste, M.; Escobar Galindo, R.; Caretti, I.; Torres, R.; Sánchez, O. Influence of the Oxygen Partial Pressure and Post-Deposition Annealing on the Structure and Optical Properties of ZnO Films Grown by Dc Magnetron Sputtering at Room Temperature. *J. Phys. D: Appl. Phys.* **2012**, *45*, 025303.

(54) Chamorro, W.; Horwat, D.; Pigeat, P.; Miska, P.; Migot, S.; Soldera, F.; Boulet, P.; Mücklich, F. Near-Room Temperature Single-Domain Epitaxy of Reactively Sputtered ZnO Films. *J. Phys. D: Appl. Phys.* **2013**, *46*, 235107.

(55) Thompson, M. W., II. The Energy Spectrum of Ejected Atoms during the High Energy Sputtering of Gold. *Philos. Mag.* **1968**, *18*, 377−414.

(56) Meyer, K. Thermalization of Sputtered Atoms. *J. Appl. Phys.* **1981**, *52*, 5803.

(57) Somekh, R. E. The Thermalization of Energetic Atoms during the Sputtering Process. *J. Vac. Sci. Technol., A: Vac. Surf. Films* **1984**, *2*, 1285.

(58) Mráz, S.; Schneider, J. M. Energy Distribution of O^- Ions during Reactive Magnetron Sputtering. *Appl. Phys. Lett.* **2006**, *89*, 051502.

(59) Mahieu, S.; Depla, D. Correlation between Electron and Negative O^- Ion Emission during Reactive Sputtering of Oxides. *Appl. Phys. Lett.* **2007**, *90*, 121117.

(60) Mahieu, S.; Aeken, K.; Depla, D. Transport of Sputtered Particles Through the Gas Phase. In *Reactive Sputter Deposition*; Depla, D., Mahieu, S., Eds.; Springer Berlin Heidelberg: Berlin, Heidelberg, 2008; Vol. *109*, pp 199−227.

(61) Ellmer, K.; Welzel, T. Reactive Magnetron Sputtering of Transparent Conductive Oxide Thin Films: Role of Energetic Particle (ion) Bombardment. *J. Mater. Res.* **2012**, *27*, 765−779.

(62) Movchan, B. A.; Demchishin, A. V. Study of the Structure and Properties of Thick Vacuum Condensates of Nickel, Titanium, Tungsten, Aluminium Oxide and Zirconium Dioxide. *Phys. Met. Metallogr.* **1969**, *28*, 83−90.

(63) Van Aeken, K.; Mahieu, S.; Depla, D. The Metal Flux from a Rotating Cylindrical Magnetron: A Monte Carlo Simulation. *J. Phys. Appl. Phys.* **2008**, *41*, 205307.

(64) Demazeau, G.; Buffat, B.; Ménil, F.; Fournès, L.; Pouchard, M.; Dance, J. M.; Fabritchnyi, P.; Hagenmuller, P. Characterization of Six-Coordinated Iron (V) in an Oxide Lattice. *Mater. Res. Bull.* **1981**, *16*, 1465−1472.

(65) Etourneau, J.; Portier, J.; Ménil, F. The Role of the Inductive Effect in Solid State Chemistry: How the Chemist Can Use It to Modify Both the Structural and the Physical Properties of the Materials. *J. Alloys Compd.* **1992**, *188*, 1−7.

(66) Kurzman, J. A.; Misch, L. M.; Seshadri, R. Chemistry of Precious Metal Oxides Relevant to Heterogeneous Catalysis. *Dalton Trans.* **2013**, *42*, 14653.

(67) Demazeau, G.; Marbeuf, A.; Pouchard, M.; Hagenmuller, P. Sur Une Série de Composés Oxygènes Du Nickel Trivalent Derivés de La Perovskite. *J. Solid State Chem.* **1971**, *3*, 582−589.

(68) Garcia, J.; Beltrán, D.; Sapiña, F.; Sanchis, M. J. Synthesis and Characterization of $NdNiO_3$ Prepared by Low Temperature Methods. *J. Alloys Compd.* **1992**, *188*, 170−173.

(69) Barbee, T. W.; Holmes, W. H.; Keith, D. L.; Pyzyna, M. K.; Ilonca, G. Synthesis of Amorphous Niobium-Nickel Alloys by Vapor Quenching. *Thin Solid Films* **1977**, *45*, 591−599.

(70) Yagi, E.; Hasiguti, R. R.; Aono, M. Electronic Conduction above 4 K of Slightly Reduced Oxygen-Deficient Rutile TiO_{2-x}. *Phys. Rev. B* **1996**, *54*, 7945.

(71) Shoko, E.; Smith, M. F.; McKenzie, R. H. Charge Distribution and Transport Properties in Reduced Ceria Phases: A Review. *J. Phys. Chem. Solids* **2011**, *72*, 1482−1494.

(72) Banerjee, A.; Pal, S.; Chaudhuri, B. K. Nature of Small-Polaron Hopping Conduction and the Effect of Cr Doping on the Transport Properties of Rare-Earth Manganite $La_{0.5}Pb_{0.5}Mn_{1-x}Cr_xO_3$. *J. Chem. Phys.* **2001**, *115*, 1550.

(73) Pi, L.; Zheng, L.; Zhang, Y. Transport Mechanism in Polycrystalline $La_{0.825}Sr_{0.175}Mn_{1-x}Cu_xO_3$. *Phys. Rev. B* **2000**, *61*, 8917.

(74) Blasco, J.; Castro, M.; Garcia, J. Structural, Electronic, Magnetic and Calorimetric Study of the Metal-Insulator Transition in $NdNiO_{3-Delta}$. *J. Phys.: Condens. Matter* **1994**, *6*, 5875.

(75) Zaanen, J.; Sawatzky, G. A.; Allen, J. W. Band Gaps and Electronic Structure of Transition-Metal Compounds. *Phys. Rev. Lett.* **1985**, *55*, 418−421.

(76) Torrance, J.; Lacorre, P.; Nazzal, A.; Ansaldo, E.; Niedermayer, C. Systematic Study of Insulator-Metal Transitions in Perovskites $RNiO_3$ (R=Pr,Nd,Sm,Eu) due to Closing of Charge-Transfer Gap. *Phys. Rev. B* **1992**, *45*, 8209−8212.

(77) García-Muñoz, J.; Aranda, M.; Alonso, J.; Martínez-Lope, M. Structure and Charge Order in the Antiferromagnetic Band-Insulating Phase of $NdNiO_3$. *Phys. Rev. B* **2009**, *79*.

(78) Baran, E. J. Structural Chemistry and Physicochemical Properties of Perovskite-like Materials. *Catal. Today* **1990**, *8*, 133−151.